PROTEINS: Structure, Function, and Bioinformatics 57:269–278 (2004)

Structure of an anti-DNA Fab Complexed with a Non-DNA Ligand Provides Insights into Cross-Reactivity and Molecular Mimicry

Jonathan P. Schuermann,[1] Michael T. Henzl,[2] Susan L. Deutscher,[2] and John J. Tanner[1,2,*]
[1]*Department of Chemistry, University of Missouri-Columbia, Columbia, Missouri*
[2]*Department of Biochemistry, University of Missouri-Columbia, Columbia, Missouri*

ABSTRACT **Antibodies that recognize DNA (anti-DNA) are part of the autoimmune response underlying systemic lupus erythematosus. To better understand molecular recognition by anti-DNA antibodies, crystallographic studies have been performed using an anti-ssDNA antigen-binding fragment (Fab) known as DNA-1. The previously determined structure of a DNA-1/dT_5 complex revealed that thymine bases insert into a narrow groove, and that ligand recognition primarily involves the bases of DNA. We now report the 1.75-Å resolution structure of DNA-1 complexed with the biological buffer HEPES (4-(2-Hydroxyethyl)piperazine-1-ethanesulfonic acid). All three light chain complementarity-determining regions (CDRs) and HCDR3 contribute to binding. The HEPES sulfonate hydrogen bonds to His L91, Asn L50, and to the backbone of Tyr H100 and Tyr H100A. The Tyr side-chains of L32, L92, H100, and H100A form nonpolar contacts with the HEPES ethylene and piperazine groups. Comparison to the DNA-1/dT_5 structure reveals that the dual recognition of dT_5 and HEPES requires a 13-Å movement of HCDR3. This dramatic structural change converts the combining site from a narrow groove, appropriate for the edge-on insertion of thymine bases, to one sufficiently wide to accommodate the HEPES sulfonate and piperazine. Isothermal titration calorimetry verified the association of HEPES with DNA-1 under conditions similar those used for crystallization (2 M ammonium sulfate). Interestingly, the presence of 2 M ammonium sulfate increases the affinities of DNA-1 for both HEPES and dT_5, suggesting that non-polar Fab–ligand interactions are important for molecular recognition in highly ionic solvent conditions. The structural and thermodynamic data suggest a molecular mimicry mechanism based on structural plasticity and hydrophobic interactions. Proteins 2004;57:269–278.** © **2004 Wiley-Liss, Inc.**

Key words: anti-DNA antibodies; X-ray crystallography; molecular mimicry; systemic lupus erythematosus; HEPES; isothermal titration calorimetry

INTRODUCTION

The autoimmune disease systemic lupus erythematosus (SLE) is characterized by an aberrant immune response involving antibodies (Abs) directed against nuclear antigens such as DNA, RNA, and nucleosomes.[1,2] Anti-DNA Abs have received considerable attention because they directly contribute to the kidney inflammation associated with SLE, known as lupus nephritis. Several possible mechanisms for the involvement of anti-DNA Abs in lupus nephritis have been proposed, including binding of anti-DNA Abs to DNA immobilized to the glomerular basement membrane (GBM), nucleosome-mediated anti-DNA Ab deposition in the GBM, and cross-reaction of anti-DNA Abs with non-DNA glomerular components.[2–10]

Given the involvement of anti-DNA Abs in the pathogenesis of SLE, there is great interest in elucidating the structural basis of Ab-DNA recognition, in order to identify features of anti-DNA Abs responsible for pathogenicity.[11,12] Such knowledge would undoubtedly contribute to a better molecular-level understanding of the role of anti-DNA Abs in SLE pathogenesis, thereby facilitating the development of SLE-specific drugs.[13,14] X-ray crystallography is central to this effort because high resolution structures of anti-DNA Abs complexed with DNA or other ligands provide templates for the design of novel SLE therapeutics that inhibit or disrupt the interactions between pathogenic anti-DNA Abs and self-antigens.

Given the potential of structure-based drug design, it is surprising that only two anti-DNA Abs have been characterized by high-resolution crystallographic analysis, namely, antigen-binding fragment (Fab) BV04-01, and the subject of this work, Fab DNA-1. The crystal structures of BV04-01, with and without bound $d(pT)_3$, were determined in the early 1990s[15]; and the structure of DNA-1 complexed with dT_5 was elucidated a decade later.[16] Determination of the DNA-1/dT_5 structure was a significant advance in the anti-DNA field, allowing for the first time, comparison of two Fab/oligonucleotide complex structures.

Abbreviations: Ab, antibody; Fab, antigen binding fragment; CDR, complementarity determining region; SLE, systemic lupus erythematosus; GBM, glomerular basement membrane; PDB, protein data bank; V, variable; C, conserved; H, heavy; L, light; RMSD, root-mean-square difference; HEPES, 4-(2-Hydroxyethyl)piperazine-1-ethanesulfonic acid; ITC, isothermal titration calorimetry.

*Correspondence to: John J. Tanner, Department of Chemistry, University of Missouri-Columbia, Columbia, MO 65211. E-mail: tannerjj@missouri.edu

Received 5 February 2004; Accepted 24 March 2004

Published online 11 June 2004 in Wiley InterScience (www.interscience.wiley.com). DOI: 10.1002/prot.20200

This comparison led to the identification of a common ssDNA recognition motif having three components: a Tyr side-chain at light (L) chain position L32, a polar side-chain at residue L91 (Ser or His), and an aromatic residue (Tyr or Trp) from the tip of HCDR3.[16] The aromatic residues from L32 and HCDR3 stack above and below the thymine base, which perfectly positions the base to form hydrogen bonds with L91. The presence of these Fab–DNA interactions in both structures suggested to us that this triad of residues is an important structural determinant of Ab–ssDNA recognition.[16]

As part of our ongoing studies of anti-DNA Ab structure and function, we now report the crystal structure of Fab DNA-1 complexed with the biological buffer molecule HEPES (4-(2-Hydroxyethyl)piperazine-1-ethanesulfonic acid). DNA-1 is a recombinant anti-ssDNA Fab that was isolated from a combinatorial bacteriophage display library of IgG fragments derived from the immunoglobulin repertoire of an autoimmune SLE-like MRL/lpr mouse.[17] This Fab displays a strong preference for binding thymine-rich ssDNA ligands with no detectable binding to dsDNA.[18,19] DNA-1 is very similar to 11F8[20–22] in terms of CDR sequence, binding thermodynamics, and base preference. This relationship is significant because 11F8 is pathogenic based on the observation that it localizes to kidney tissue by binding to DNA adherent to the GBM.[6] While it remains to be seen whether DNA-1 also displays pathogenic behavior, the similarities to 11F8 suggest that crystallographic studies of DNA-1 will likely provide insights into how a pathogenic anti-DNA Ab recognizes ligands.

The DNA-1/HEPES crystal structure reported here reveals that HEPES binds in the previously characterized dT_5 binding site, and that several of the residues responsible for dT_5 recognition also participate in binding HEPES. Large conformational changes in HCDR3 allow DNA-1 to bind, separately, ssDNA and HEPES. These results illustrate the structural plasticity of the DNA-1 Fab, demonstrating the dramatic rearrangement of an anti-DNA combining site to accommodate a non-DNA ligand. This finding implies a major role for protein flexibility in anti-DNA Ab cross-reactivity.

MATERIALS AND METHODS

Crystallization and X-ray Data Collection

The details of recombinant protein expression and purification have been reported elsewhere.[23] The crystal used for data collection was grown in a sitting drop at 22°C over a reservoir of 0.1 M HEPES, 1.85 M ammonium sulfate, 2% PEG 400, pH 8.1. The sitting drop was formed by mixing equal volumes of the reservoir and a stock solution of 18 mg/mL Fab DNA-1 in 10 mM Tris HCl, 50 mM NaCl (pH 7.0). The space group is $P2_12_12$ with cell dimensions a = 107.7 Å, b = 156.7 Å, c = 61.0 Å, and the asymmetric unit contains two Fabs with a solvent content of 51%.

The crystal was prepared for cryogenic X-ray data collection by replacing the mother liquor with solutions of the harvest buffer (0.1 M HEPES, 2M ammonium sulfate, 2% PEG 400, pH 8.0) supplemented with increasing amounts of glycerol. The glycerol concentration was raised from zero to 30% in increments of 5% over a period of about 10 min, and then the crystal was plunged into liquid nitrogen.

The frozen crystal was transported to the National Synchrotron Light Source at Brookhaven National Laboratory for data collection. X-ray diffraction data were collected to 1.75-Å resolution at beamline X8C. A scan of 108° of data was collected using a Quantum 4 CCD detector with an oscillation angle of 0.5°, an exposure time of 3.67 min per degree of oscillation, a detector distance of 130 mm, and a detector 2θ angle of zero. The data were integrated with *HKL2000* and merged with *HKL*.[24] The reflection intensities were converted to amplitudes with the method of French and Wilson[25] as implemented in CCP4.[26] See Table I for data collection statistics.

Molecular Replacement, Model Building, and Refinement

Molecular replacement calculations were performed with AMoRe[27] using a search model extracted from the previously solved structure of Fab DNA-1 bound to dT_5 (PDB entry 1I8M).[16] A clear solution for two Fabs in the asymmetric unit was identified, with a correlation coefficient of 63.3% and an R-factor of 0.41.

Following molecular replacement, rigid body refinement was performed using CNS.[28] In preparation for positional refinement and model building sessions in O,[29] the CDR loops were omitted from the model. The Engh and Huber force field[30] and the maximum likelihood amplitude target were used in CNS refinement. Prior to each round of CNS refinement, an overall anisotropic B-value correction was applied to the data and a bulk solvent correction was calculated. Simulated annealing was used in the first round of refinement, and conjugate gradient minimization was used in subsequent rounds. Individual atomic B-factor refinement was performed after positional refinement. Cross validation was used with a randomly chosen test set of 9796 reflections and a working set of 88,140 reflections. Non-crystallographic symmetry restraints were not used in refinement due to the high resolution of the data.

The CDR loops were gradually built as the quality of the maps improved. Once the protein structure was nearly complete and the R-factor dropped below 0.28, water molecules were added using the automated water picking routine of CNS. Water sites were filled if they displayed at least a 3σ peak in the F_o–F_c map and possessed good hydrogen bonding. Water molecules were inspected after refinement, and they were deleted if they displayed weak or nonspherical $2F_o$–F_c density viewed at the 1σ level. Close inspection of the electron density resulted in the incorporation of nine sulfate ions, two HEPES molecules, six PEG fragments, and sixteen glycerol molecules.

The occupancies of the two HEPES molecules and the two sulfate ions bound to the CDRs were estimated from alternating cycles of B-factor and occupancy refinement, using the method suggested by Jensen.[31] These calculations resulted in occupancy values of 0.95 for the two HEPES molecules, 0.91 for the sulfate ion bound to Fab 1,

TABLE I. Data Collection and Refinement Statistics

Wavelength (Å)	0.97950
Space group	$P2_12_12$
Unit cell dimensions (Å)	$a = 107.7, b = 156.7, c = 61.0$
Number of crystals	1
Number of Fabs per asymmetric unit	2
Diffraction resolution (Å)	100–1.75 (1.81–1.75)[a]
Number of observations	338, 206
Number of unique reflections	98, 022
Redundancy	3.5
Completeness (%)	93.5 (94.1)[a]
Mean I/σ_1	21.7 (2.1)[a]
R_{merge}	0.044 (0.487)[a]
Number of protein atoms	6,551
Number of water molecules	786
Number of HEPES molecules	2
Number of sulfate ions	9
Number of glycerol molecules	16
Number of PEG molecules	6
R_{cryst}	0.197 (0.294)
R_{free}[b]	0.230 (0.316)
RMSD[c]	
Bond lengths (Å)	0.010
Bond angles (degree)	1.72
Dihedral angles (degree)	27.7
Improper dihedrals (degree)	0.955
Ramachandran plot[d]	
Favored (%)	89.5
Allowed (%)	9.7
Generous (%)	0.5
Disallowed (%)	0.3
Average *B*-factors (Å^2)	
Protein	26
Solvent	43

[a]Values for the outer resolution shell of data are given in parenthesis.
[b]10% R_{free} test set.
[c]Compared to the Engh and Huber force field.[30]
[d]The Ramachandran plot was generated with PROCHECK.[37]

and 0.87 for the sulfate ion bound to Fab 2. These results suggest that the HEPES and sulfate ligands are present at nearly unit occupancy.

Coordinates and structure factors have been deposited in the PDB[32] as entry 1P7K.

Isothermal Titration Calorimetry

Anticipating a low affinity interaction between HEPES and DNA-1, the competition-based ITC method described by Zhang and Zhang was used to measure the association constant and enthalpy of HEPES binding to DNA-1.[33] Basically, the binding of a high-affinity ligand (dT_5 in this case) is monitored in the absence and presence of the low-affinity ligand (HEPES in this case). The binding parameters for the low-affinity ligand are then extracted from the resulting data sets with the following equations,[33]

$$K_{HEP} = (K_{dT5}/K_{app} - 1)/[HEP]_{tot} \quad (1)$$

$$\Delta H_{HEP} = (\Delta H_{dT5} - \Delta H_{app})(1 + 1/K_{HEP}/[HEP]_{tot}) \quad (2)$$

where K_{dT5} and K_{app} are the association constants for the binding of dT_5 to DNA-1 in the absence and presence of HEPES, respectively, ΔH_{dT5} and ΔH_{app} are the enthalpies for dT_5 binding to DNA-1 in the absence and presence of HEPES, respectively, and $[HEP]_{tot}$ is the total concentration of HEPES present in the second titration. This method is appropriate because our crystal structures have established that HEPES and dT_5 compete for the same binding site.

All ITC experiments were performed in a MicroCal VP-ITC at 25°C. The dT_5 was purchased from either Sigma-Genosys (HPLC purified) or Integrated DNA Technologies (standard desalting preparation) and used without further purification. For each titration, DNA-1, at a concentration of 0.03 mM, was placed in the calorimeter cell, and dT_5 (1.2–1.3 mM) was added to the cell via the rotating stirrer-syringe. Four titrations were performed, corresponding to the following buffers: (1) 0.01 M imidazole, 0.1 M NaCl (pH 7.0); (2) 0.01 M imidazole, 0.1 M Na HEPES (pH 7.0); (3) 0.01 M imidazole, 0.1 M NaCl (pH 7.0), 2 M $(NH_4)_2SO_4$; (4) 0.01 M imidazole, 0.1 M Na HEPES (pH 7.0), 2 M $(NH_4)_2SO_4$. Prior to each titration, separate solutions of ligand and protein were dialyzed exhaustively into the same buffer. The two $(NH_4)_2SO_4$

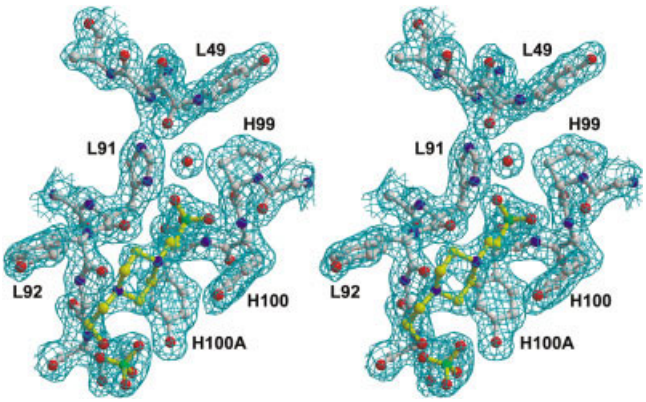

Fig. 1. Stereo-view of a 2Fo–Fc electron density map (1σ) draped over the final model. Phases for the map calculation were determined from the final model. Chemical bonds of the protein are colored white, while those of the HEPES and sulfate ligands are colored yellow. The orientation of the protein depicted in this figure is identical to those of Figure 3 and 4. This figure was prepared with Bobscript[55] and Raster3D.[56]

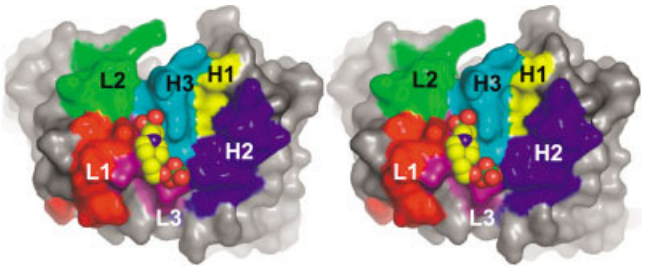

Fig. 2. Stereo-view of the HEPES binding site highlighting CDR usage. The protein is depicted as a solvent accessible surface, while the HEPES and sulfate ligands are drawn as CPK spheres. The CDRs are color coded as follows: LCDR1-red, LCDR2-green, LCDR3-purple, HCDR1-yellow, HCDR2-blue, and HCDR3-cyan. This and other figures were prepared with Pymol.[57]

buffers were titrated to pH = 7.0 before adding $(NH_4)_2SO_4$. Values of the association constant and enthalpy were obtained by fitting the integrated heats of association to the one-site binding model using the software supplied with the instrument. The results were corrected for the heat of mixing and ligand dilution, which was measured for each titration by injecting dT_5 (1.3 mM) into the appropriate buffer devoid of protein.

RESULTS

Description of the Overall Structure and Nomenclature

The Fab crystal structure presented here was determined using a 1.75-Å resolution X-ray diffraction data set collected from a single crystal using synchrotron radiation. Thus, it is the highest-resolution anti-DNA Fab structure solved to date and provides our most accurate view so far of an anti-DNA Ab combining site. The electron density was of exceptional quality (Fig. 1) and allowed unambiguous modeling of the entire protein main-chain except for heavy (H) chain residues 127–133, which are disordered in many Fab structures, including the DNA/dT_5 structure.[16] The R-factor for the refined model is 0.197, with an R-free[34] (10% test set) of 0.230. A Luzzati plot[35] suggests a mean positional error of 0.21 Å, while the σ_A error estimate[36] is 0.19 Å. The structure exhibits good stereochemical quality that is consistent with 1.75-Å resolution data (Table I), and it meets or exceeds all main-chain and side-chain tests of PROCHECK.[37]

The asymmetric unit contains two Fabs (Fab 1 and Fab 2), with the light (L) and heavy (H) chains denoted L and H in Fab 1, and A and B in Fab 2. The residue-numbering scheme and CDR definitions follow the standard Kabat conventions.[38,39] Both Fabs display the expected immunoglobulin fold in which each of the four homology subunits, denoted V_H, V_L, C_H1, and C_L, consists of two twisted, antiparallel β sheets packed tightly against each other.[40,41] The two Fab structures are very similar to each other in terms of both the polypeptide conformation throughout the Fabs and the quaternary structure. The root mean square difference (RMSD) between the two Fabs, after superimposing the main-chains, is 0.41 Å for the main-chain and 0.52 Å for all atoms. The RMSD for the V_H/V_L superdomain is 0.32 Å for the main-chain and 0.44 Å for all atoms, while the analogous values for the C_H1/C_L superdomain are 0.39 Å for the main-chain and 0.51 Å for all atoms. The two Fabs have similar elbow angles (168°, 171°).

Fab–Ligand Interactions

The original goal of the present study was to elucidate a structure of the unliganded Fab, and so ssDNA was not added to the protein solution prior to crystallization. However, electron density maps clearly indicated the presence of two small molecule ligands bound to the complementarity-determining regions (CDRs) near the previously established oligo(dT) binding sites of both Fabs (Fig. 1). The excellent quality of the 1.75-Å resolution maps allowed us to assign these features to a molecule of the zwitterionic buffer HEPES and to a sulfate ion. Note that the crystallization reservoir contained 0.1 M HEPES and approximately 2 M $(NH_4)_2SO_4$ and that equal amounts of the protein stock solution and reservoir were mixed to form sitting drops for crystallization. It is possible that the bound sulfate ion could represent the sulfonate group of a second HEPES molecule, based on the presence of weak electron density connected to the modeled sulfate ion. However, the density was not sufficiently convincing to support inclusion of a second HEPES and was therefore modeled as a sulfate ion instead. The HEPES and sulfate ligands were found in both Fabs, and the protein–ligand interactions were nearly identical in both Fabs. Thus, the discussion below will be restricted to Fab 1.

The HEPES molecule binds in a pocket formed by all three L chain CDRs and HCDR3 (Fig. 2). The total surface area buried in the Fab/HEPES interface is 537 $Å^2$, with the protein and HEPES contributing 269 $Å^2$ and 268 $Å^2$, respectively.[42] The burial of 268 $Å^2$ of surface area by HEPES amounts to 64% of its total solvent accessible surface area. The L and H chains contribute almost equally to the protein side of the interface. LCDR1 and LCDR3 account for 16% and 37% of the protein side of the interface, respectively. HCDR3 contributes 47% of the

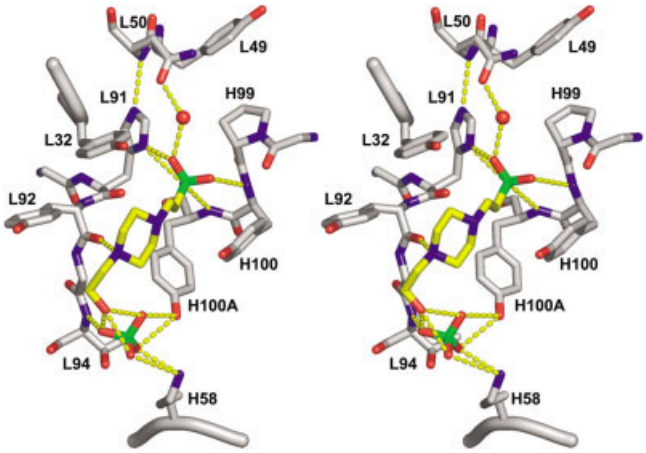

Fig. 3. Stereo-view of the DNA-1/HEPES binding site highlighting Fab–ligand interactions. The HEPES and sulfate ligands appear in yellow and green; protein side-chains are colored white. The dotted lines denote hydrogen bonds and ion pairs. The orientation of the protein depicted in this figure is identical to those of Figures 1 and 4.

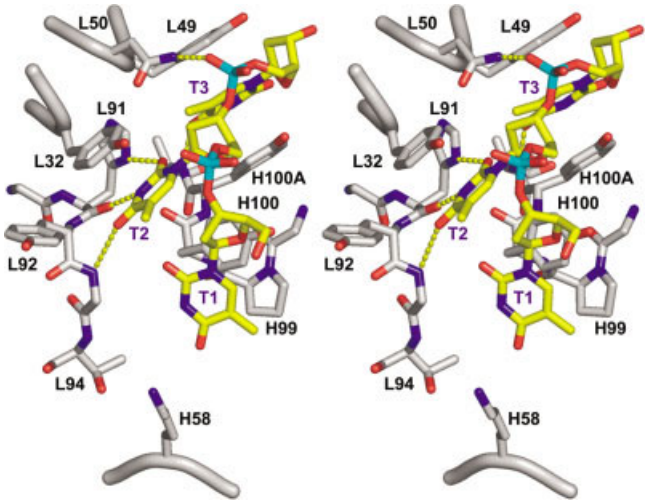

Fig. 4. Stereo-view of Fab-DNA interactions from DNA-1/dT_5 structure (PDB code 1I8M).[16] DNA appears in yellow, while protein side-chains are colored white. The dotted lines denote hydrogen bonds. The orientation of the protein depicted in this figure is identical to those of Figures 1 and 3.

protein side of the interface. Although the surface area analysis suggests that LCDR2 does not participate in the binding of HEPES, Asn L50 of LCDR2 contributes a water-mediated hydrogen bond to the HEPES sulfonate (see discussion below).

The HEPES sulfonate binds in a pocket located at the intersection of LCDR1, LCDR2, LCDR3, and HCDR3. The sulfonate accepts two hydrogen bonds from the side-chain of His L91, and two hydrogen bonds from the backbone N-H groups of Tyr H100 and Tyr H100A (Fig. 3). The ionization state of His L91 appears to be neutral rather than cationic because an imidazole N atom of His 91 is perfectly positioned to accept a hydrogen bond from the backbone N-H of Asn L50 (NE2-N distance of 3.1 Å). Thus, the interaction between His L91 and the sulfonate is probably a hydrogen bond rather than an ion pair. Asn L50 participates in the stabilization of HEPES by forming a water-mediated hydrogen bond with the sulfonate (Fig. 3). The density representing this water molecule is quite strong (Fig. 1), and the refined B-value of 23 $Å^2$ is well below the average solvent B-value of 39 $Å^2$, which indicates that this water-mediated hydrogen bond is a significant interaction.

While the sulfonate binding pocket appears to be the main recognition locus, there are many nonpolar and polar interactions formed between the Fab and the nonsulfonate parts of the HEPES. These other interactions distinguish HEPES from a sulfate ion, and the binding of HEPES, present at 0.1 M, in the presence of 2 M sulfate ion, attests to their importance. These interactions with the nonsulfonate moieties include several nonpolar protein–ligand contacts help stabilize the bound HEPES by providing shape complementarity and favorable van der Waals interactions. For example, the ethylene linker between the sulfonate and piperazine groups contacts side-chain C atoms of Tyr H100 and Tyr H100A, while the piperazine contacts C atoms of Tyr H100A, Tyr L32, and Tyr L92 (Fig. 3). The piperazine ring adopts a chair conformation, with the carbonyl bond of Tyr L92 oriented perpendicular to the face of the piperazine ring (Fig. 3). This arrangement brings the carbonyl O atom within 2.8 Å of the piperazine N2. Thus, there appears to be a hydrogen bond between the carbonyl and the piperazine N2, with the latter presumably protonated.

Finally, the HEPES hydroxyl forms three hydrogen bonds to a sulfate ion (possibly the sulfonate of a second HEPES) that is also bound by the Fab. The sulfate forms an ion pair with Lys H58 of HCDR2, and it hydrogen bonds to Thr L94 and Tyr H100A (Fig. 3). The average B-factor of the HEPES is 38 $Å^2$ with the HEPES sulfonate having an average B-factor of only 26 $Å^2$. In contrast, the B-factor of the bound sulfate ion is higher, 43 $Å^2$.

Comparison to the DNA-1/dT_5 Structure

The structure of DNA-1 complexed to the ssDNA ligand dT_5 was previously determined at 2.1 Å resolution.[16] The dT_5 ligand binds in a narrow groove formed by all three L chain CDRs and HCDR3, and most of the Fab–DNA interactions involve the bases of the second and third nucleotides (T2 and T3) of the dT_5 ligand. On the protein side, the important residues are Tyr L32, Tyr L49, Asn L50, His L91, Tyr L92, Tyr H100, and Tyr H100A (Fig. 4). These Tyr side-chains line the binding groove and form van der Waals interactions with the thymine bases. The base of T2 is sandwiched between the aromatic rings of Tyr L32 and Tyr H100, while His L91 hydrogen bonds to a carbonyl of the T2 thymine base. Similarly, the base of T3 is sandwiched between the side-chains of Tyr L49 and Tyr H100A, and the base hydrogen bonds to the backbone of Ala H100B. Asn L50 provides the lone interaction with the DNA backbone by hydrogen-bonding to the phosphate moiety between T2 and T3. Importantly, the triad of L32, L91, and H100 has been hypothesized to be particularly important for ssDNA–antibody recognition, based on its

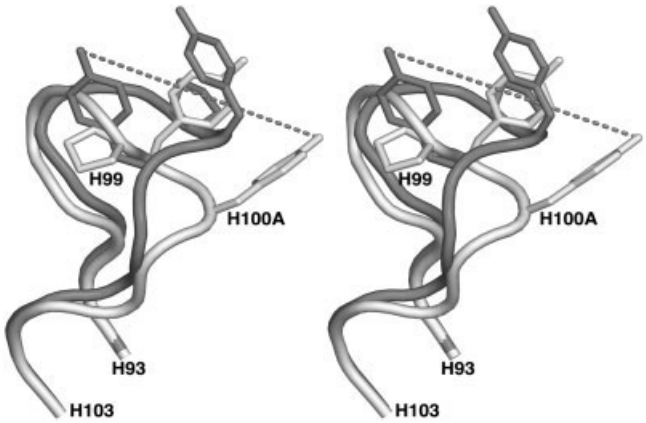

Fig. 5. Stereo-view of HCDR3 conformations from the DNA-1/HEPES (light) and DNA-1/dT_5 (dark) structures. The side-chains of Pro H99, Tyr H100, and Tyr H100A are shown for both structures. The residue labels refer to the DNA-1/HEPES structure. The dashed line denotes the 13-Å difference in the positions of Tyr H100A in the two structures.

appearance in both the BV04-01/ $d(pT)_3$ and DNA-1/dT5 structures.[16]

The HEPES and dT_5 binding sites of DNA-1 are remarkably similar in terms of CDR usage and the identities of residues that contact the ligands, despite the obvious chemical and structural differences between the two ligands. For example, in both the DNA-1/dT_5 and DNA-1/HEPES structures, the ligand-binding site consists of residues from all three L chain CDRs plus HCDR3, with no contributions from HCDR1. The side-chains of Tyr L32, Tyr L92, Tyr H100, and Tyr H100A line both binding sites. These aromatic rings in both complexes help to align the ligand in the binding site so that Asn L50 and His L91 can hydrogen-bond to the ligand. Finally, note that the critical triad of Tyr L32, His L91, and Tyr H100 is used for ligand recognition in both structures.

Despite the aforementioned similarities, the dT_5 and HEPES binding sites differ in terms of shape and size, and these important differences are due to large conformational changes in HCDR3. The RMSD between the HCDR3 loops of the DNA-1/dT_5 and DNA-1/HEPES structures is 2.2 Å for the main-chain and 4.4 Å for all atoms (following superposition of the HCDR3 main-chain). For reference, the main-chain RMSD for the entire V_H/V_L superdomain is only 0.8 Å, while the main-chain RMSDs for the other five CDRs are less than 0.7 Å. The largest conformational differences in HCDR3 involve Pro H99, Tyr H100, and Tyr H100A, which are located in the tip of the loop (Fig. 5). The conformational change in HCDR3 results in movements of 10 Å for Pro H99 (based on the CG atom), 4 Å for Tyr H100 (based on the hydroxyl), and 13 Å for Tyr H100A (based on the hydroxyl).

The structural changes of HCDR3 modify the size and shape of the binding site to match the size and shape requirements of the ligand. In the DNA-1/dT_5 complex, the binding site is a narrow groove, just wide enough to accommodate the edge-on insertion of thymine bases T2 and T3 (Fig. 4). The width is 7 Å, as measured by the distance between the side-chains of Tyr 32 and Tyr H100, or between Tyr L49 and Tyr H100A. This groove, however, is too narrow for the sulfonate group of HEPES, thus necessitating a conformational change in the protein. The structural rearrangement of HCDR3 widens the T2 binding site by 2–3 Å, which creates a pocket big enough for the sulfonate. Another consequence of the HCDR3 movement is that the T3 site is occluded because of the movement of Pro H99 into van der Waals contact with Tyr H49 (Fig. 3). Thus, the ability of DNA-1 to recognize both oligo(dT) and HEPES is critically dependent on the flexibility of HCDR3.

Isothermal Titration Calorimetry

The discovery of a HEPES molecule bound to DNA-1 in the crystal structure prompted us to examine the binding of HEPES to DNA-1 in solution using ITC. Anticipating a low affinity interaction, competition ITC experiments were used to measure the apparent affinity of DNA-1 for a high-affinity ligand, dT_5, in the absence and presence of 0.1 M Na HEPES. Figure 6(a) shows the results for a titration performed in 0.01 M imidazole, 0.1 M NaCl (pH 7.0). The apparent association constant, obtained by fitting the integrated heats of injection to the one-site binding model, is $K_A = 6.0 \times 10^4\ M^{-1}$ (Table II). This value agrees well with that measured previously using fluorescence quenching under similar buffer conditions ($K_A = 3.7 \times 10^4$).[43] The binding of dT_5 to DNA-1 is exothermic, with an apparent ΔH_{cal} under our solution conditions of −16.8 kcal/mol. Although the calorimetric enthalpy had not been previously measured, an estimate of the van't Hoff enthalpy (−25 kcal/mol, 50 mM Tris, pH 7.0) had been extracted previously from fluorescence quenching data for the binding of dT_5 to DNA-1.[19] Thus, our ITC data display reasonable agreement with existing thermodynamic data for DNA-1.

The effect of HEPES on the binding of dT_5 to DNA-1 is shown in Figure 6(b). The conditions of this titration were identical to those of Figure 6(a), except that 0.1 M Na HEPES was substituted for 0.1 M NaCl in the buffers used for both the dT_5 and DNA-1 solutions. The presence of HEPES caused a slight decrease in the affinity constant, to $K_A = 4.9 \times 10^4\ M^{-1}$, and a slight lowering of the enthalpy to −18.5 kcal/mol. Using Equations (1) and (2), the thermodynamic parameters for HEPES binding to DNA-1 are $K_A = 2.4\ M^{-1}$ and $\Delta H = 8.7$ kcal/mol. Note that the enthalpy of HEPES binding to DNA-1 in low salt conditions is endothermic.

ITC experiments were also performed in the presence of 2 M $(NH_4)_2SO_4$, in order to mimic the conditions used for crystallization. These results are shown in Figure 7. Surprisingly, the presence of 2 M $(NH_4)_2SO_4$ increased the affinity of DNA-1 for dT_5 twofold, to $K_A = 1.3 \times 10^5\ M^{-1}$ [Fig. 7(a); Table II]. In addition, the presence of $(NH_4)_2SO_4$ increased the exothermicity of the binding to $\Delta H = -21.4$ kcal/mol [Fig. 7(a); Table II]. The ITC results performed in the presence of both 2 M $(NH_4)_2SO_4$ and 0.1 M Na HEPES are shown in Figure 7(b). From Equations (1) and (2), the thermodynamic parameters for HEPES binding to DNA-1 in the presence of 2 M $(NH_4)_2SO_4$ are $K_A = 5.7\ M^{-1}$ and $\Delta H = -7.0$ kcal/mol (Table II). As with dT_5, the presence of

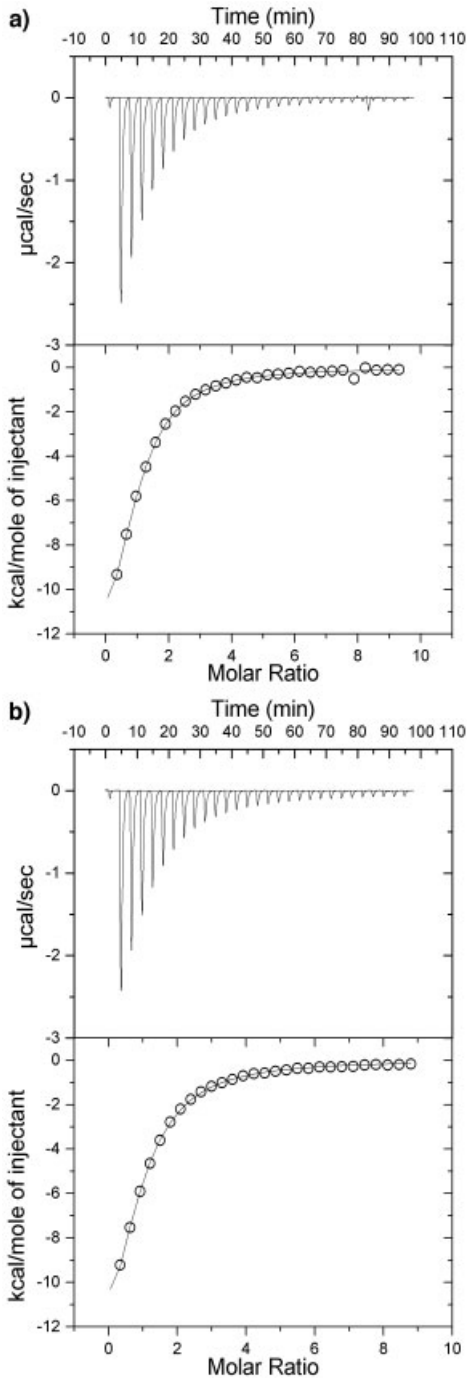

Fig. 6. ITC analysis of dT_5 binding to Fab DNA-1 in low salt buffers. The upper panel of each figure shows the raw calorimetric data, and the lower panel shows the corresponding integrated injection heats, corrected for the heat of dilution. The curves in the lower halves of each figure represent the best least-squares fits to the one-site binding model. **a**: Prior to titration, dT_5 and DNA-1 were dialyzed separately into 0.01 M imidazole, 0.1 M NaCl (pH 7.0). The apparent thermodynamic parameters from the best fit curve are $K = 6.0 \times 10^4 \pm 0.3 \times 10^4\ M^{-1}$, $\Delta H = -16.8 \pm 0.7$ kcal/mol. **b**: Prior to titration, dT_5 and DNA-1 were dialyzed separately into 0.01 M imidazole, 0.1 M Na HEPES (pH 7.0). The apparent thermodynamic parameters from the best fit curve are $K = 4.9 \times 10^4 \pm 0.1 \times 10^4\ M^{-1}$, $\Delta H = -18.5 \pm 0.4$ kcal/mol.

TABLE II. Isothermal Titration Calorimetry Data for Ligand Binding to Fab DNA-1 at 298 K

Ligand	$[(NH_4)_2SO_4)]$	$K\ (M^{-1})$	ΔH (kcal/mol)	$-T\Delta S$ (kcal/mol)
dT_5	0	6.0×10^4	−16.8	10.3
dT_5	2	1.3×10^5	−21.4	14.4
HEPES	0	2.4	8.7	−9.2
HEPES	2	5.7	−7.0	5.9

2 M $(NH_4)_2SO_4$ increased the affinity of DNA-1 for HEPES. Note also that 2 M $(NH_4)_2SO_4$ decreased the apparent enthalpy of HEPES binding to DNA-1 and that the association is now exothermic with an unfavorable entropy change (Table II).

DISCUSSION

This paper reports the first crystal structure of an anti-DNA Fab complexed with a non-DNA ligand. Together with the DNA-1/dT_5 structure, the current structure provides a three-dimensional framework for understanding cross-reactivity and molecular mimicry in the context of anti-DNA Abs. Several studies have reported the binding of non-DNA ligands to anti-DNA Abs, including anionic dyes,[44] benzodiazepines,[7] pneumococcal polysaccharide,[45] phosphorylcholine,[45,46] the protein α-actinin,[47] acidic pentapeptides,[48] the NR2 glutamate receptor,[49] Cys-constrained 16-mer peptides,[50] histones,[50] and nucleosomes.[2,50] Thus, the ability to recognize multiple ligands is a hallmark of anti-DNA Abs. Molecular mimicry is one mechanism by which autoimmune diseases can occur in association with infectious agents.[51] This idea presumes that foreign antigens trigger an immune response, and that the antibodies produced cross-react with host molecules that are structurally and chemically similar to the triggering antigen. For example, in the case of SLE pathogenesis, phosphorylcholine (PC), a component of pneumococcal cell wall polysaccharide, has been proposed as a triggering antigen, with the phosphate moiety of PC presumably mimicking the phosphate backbone of self-antigen DNA.[46,52,53]

The work presented here affords an opportunity to examine how an anti-DNA Ab recognizes similar features on different molecules, which is germane to the notions of cross-reactivity and molecular mimicry. HEPES contains a sulfonate group, analogous to the phosphate group of the DNA backbone. Based on the simple notion of molecular mimicry, one would predict these two groups to form similar interactions with the Fab. The sulfonate hydrogen-bonds to His L91, the main-chain of H100 and H100A, and to a water molecule. The major interaction partner with the sulfonate appears to be His L91 (Fig. 3). This residue hydrogen bonds to a thymine base in the DNA-1/dT_5 structure; it makes no interactions with the DNA backbone (Fig. 4). Thus, molecular mimicry based on the similarity of sulfonate to the phosphate of DNA does not explain the recognition of HEPES by DNA-1. On the other hand, both DNA-1 structures show a hydrophobic ring of the ligand bound between Tyr side-chains (Figs. 3, 4),

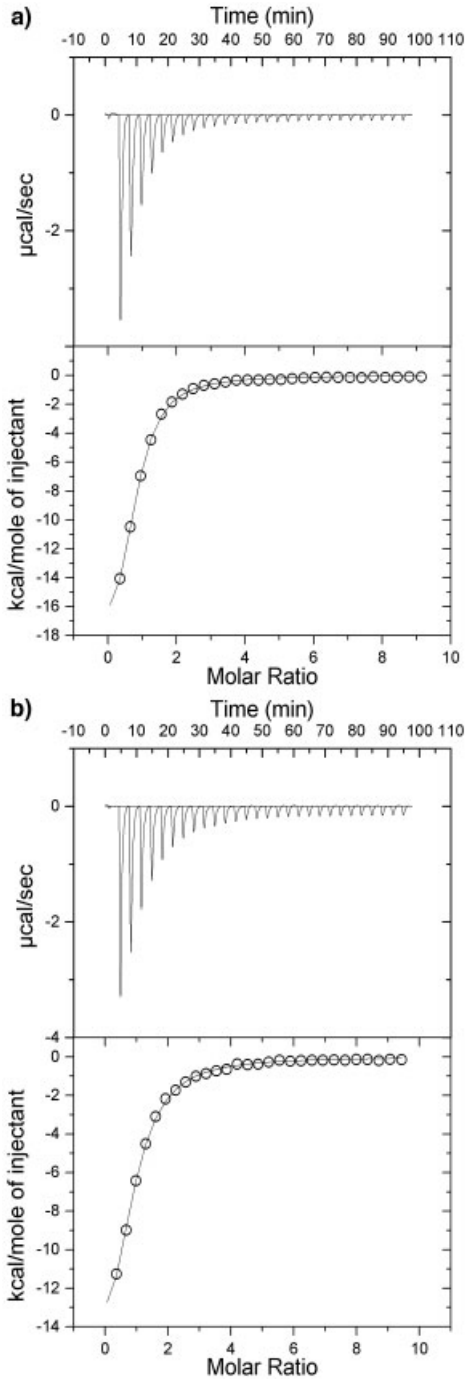

Fig. 7. ITC analysis of dT_5 binding to Fab DNA-1 in 2 M $(NH_4)_2SO_4$ buffers. The upper panel of each figure shows the raw calorimetric data, and the lower panel shows the corresponding integrated injection heats, corrected for the heat of dilution. The curves in the lower halves of each figure represent the best least-squares fits to the one-site binding model. **a**: Prior to titration, dT_5 and DNA-1 were dialyzed separately into 0.01 M imidazole, 0.1 M NaCl, 2 M $(NH_4)_2SO_4$ (pH 7.0). The apparent thermodynamic parameters from the best fit curve are $K = 1.3 \times 10^5 \pm 0.04 \times 10^5$ M^{-1}, $\Delta H = -21.4 \pm 0.4$ kcal/mol. **b:** Prior to titration, dT_5 and DNA-1 were dialyzed separately into 0.01 M imidazole, 0.1 M Na HEPES, 2 M $(NH_4)_2SO_4$ (pH 7.0). The apparent thermodynamic parameters from the best fit curve are $K = 8.3 \times 10^4 \pm 0.3 \times 10^4$ M^{-1}, $\Delta H = -18.9 \pm 0.5$ kcal/mol.

which suggests a molecular mimicry mechanism based on hydrophobic interactions rather than ionic interactions.

It is significant that Tyr L32, His L91, and Tyr H100 participate directly in the recognition of HEPES. These residues are also very important for binding oligo(dT), based on the crystal structures of DNA-1/dT_5 and BV04-01/ $d(pT)_3$. This triad of residues, therefore, possibly form a ligand recognition "hot spot," rather than a ssDNA-specific recognition motif, as was proposed earlier.[16] Future structural and mutagenesis studies of Fab DNA-1 will test this hypothesis.

The DNA-1/HEPES structure provides a basis for interpreting early work that examined the binding of low molecular weight anionic compounds to anti-DNA Abs.[44] Several organic compounds, such as synthetic dyes like acid magenta, FD and C Green No. 3, and methyl blue, were tested for their ability to inhibit the binding of *Escherichia coli* native DNA to the NZB/NZW monoclonal anti-DNA Ab A52, which binds both ssDNA and dsDNA. Interestingly, only compounds displaying an anionic functional group inhibited DNA association. Moreover, the best inhibitors featured a sulfonate group bound to a six-membered aromatic ring.

It is tempting to think that these anionic inhibitors might bind to A52 in a way that is analogous to the binding of HEPES to DNA-1. This notion is supported by sequence analysis. The A52 L chain contains, like DNA-1, Tyr L32, His L91, and Tyr L92. In addition, HCDR3 of A52 features two contiguous aromatic residues (Tyr and Phe) that are analogous to Tyr H100 and Tyr H100A of DNA-1. Thus, A52 possesses most of the side-chains that DNA-1 uses to bind the sulfonate-containing ligand HEPES, and it is therefore reasonable to think that the structure presented here provides a plausible model of the A52/ligand complexes previously studied. The ITC data presented here confirm the binding of HEPES to DNA-1 in solution, although the affinity is rather low. It is interesting that the presence of 2 M $(NH_4)_2SO_4$ enhanced the binding of both HEPES and dT_5 to DNA-1. These results suggest that nonpolar Fab–ligand interactions are important for molecular recognition in highly ionic solvent conditions. This picture is consistent with the structure presented here, which shows the HEPES ligand making significant nonpolar contacts with Tyr side-chains (Fig. 3). It is also consistent with the structure of DNA-1 complexed with dT_5, which was determined from crystals grown in 2 M $(NH_4)_2SO_4$.[16] The DNA-1/dT_5 structure shows thymine bases sandwiched by Tyr side-chains, resulting in the burial of significant nonpolar surface area (Fig. 4).

The binding of HEPES to DNA-1 is reminiscent of the recent work by Stevens, Schultz, and coworkers, in which a crystallization component, jeffamine, unexpectedly bound the germline precursor to antibody 7G12.[54] The resulting Fab/jeffamine complex provided insight into how somatic mutations optimize the binding site by the reducing the structural plasticity that is necessary for binding diverse, nonhapten ligands. Similarly, we find that structural plasticity underlies the ability of DNA-1 to recognize different ligands.

Finally, the large conformational changes observed in HCDR3 suggest it is highly unlikely that theoretical modeling will provide reliable three-dimensional models of anti-DNA combining sites. Current modeling programs would certainly not have predicted the DNA-1/HEPES structure from the DNA-1/dT_5 structure, much less from sequence information alone. Thus, there remains a pressing need for more crystal structures of anti-DNA Abs.

ACKNOWLEDGMENTS

We thank Season P. Prewitt for help with protein purification, and the personnel of NSLS beamline X8C for their assistance with data collection. This research was supported, in part, by grants from the University of Missouri Research Board to J.J.T. and S.L.D. Part of this research was carried out at the National Synchrotron Light Source, Brookhaven National Laboratory, which is supported by the U.S. Department of Energy, Division of Materials Sciences and Division of Chemical Sciences, under Contract No. DE-AC02-98CH10886.

REFERENCES

1. Stollar BD. Anti-DNA antibodies. Clinics Immunol Allergy 1981;1: 243–260.
2. Amoura Z, Koutouzov S, Piette JC. The role of nucleosomes in lupus. Curr Opin Rheumatol 2000;12:369–373.
3. Pisetsky DS, Grudier JP, Gilkeson GS. A role for immunogenic DNA in the pathogenesis of systemic lupus erythematosus. Arthritis Rheum 1990;33:153–159.
4. Winfield JB, Faiferman I, Koffler D. Avidity of anti-DNA antibodies in serum and IgG glomerular eluates from patients with systemic lupus erythematosus. Associations of high avidity antinative DNA antibody with glomerulonephritis. J Clin Invest 1991;59: 90–95.
5. Murakami H, Lam Z, Furie BC, Reinhold VN, Asano T, Furie B. Sulfated glycolipids are the platelet autoantigens for human platelet-binding monoclonal anti-DNA autoantibodies. J Biol Chem 1991;266:15414–15419.
6. Swanson PC, Yung RL, Blatt NB, Eagan MA, Norris JM, Richardson BC, Johnson KJ, Glick GD. Ligand recognition by murine anti-DNA autoantibodies. II. Genetic analysis and pathogenicity. J Clin Invest 1996;97:1748–1760.
7. Blatt NB, Glick GD. Anti-DNA autoantibodies and systemic lupus erythematosus. Pharmacol Ther 1999;83:125–139.
8. Waer M. The role of anti-DNA antibodies in lupus nephritis. Clin Rheumatol Suppl 1 1990;9:111–114.
9. Isenberg DA, Ehrenstein MR, Longhurst C, Kalsi JK. The origin, sequence, structure, and consequences of developing anti-DNA antibodies. A human perspective. Arthritis Rheum 1994;37:169–180.
10. Eilat D, Anderson WF. Structure-function correlates of autoantibodies to nucleic acids. Lessons from immunochemical, genetic and structural studies. Mol Immunol 1994;31:1377–1390.
11. Rahman A, Kumar S, Potter KN. Anti-DNA antibodies—structure and function. Lupus 2002;11:776–779.
12. Jang YJ, Stollar BD. Anti-DNA antibodies: aspects of structure and pathogenicity. Cell Mol Life Sci 2003;60:309–320.
13. Jones DS, Barstad PA, Feild MJ, Hachmann JP, Hayag MS, Hill KW, Iverson GM, Livingston DA, Palanki MS, Tibbetts AR, et al. Immunospecific reduction of antioligonucleotide antibody-forming cells with a tetrakis-oligonucleotide conjugate (LJP 394), a therapeutic candidate for the treatment of lupus nephritis. J Med Chem 1995;38:2138–2144.
14. Linnik M, Staines NA, Berden J, Isenberg DA. Workshop report on some new ideas about the treatment of systemic lupus erythematosus. Lupus 2002;11:793–796.
15. Herron JN, He XM, Ballard DW, Blier PR, Pace PE, Bothwell ALM, Voss Jr. EW, Edmundson AB. An autoantibody to single-stranded DNA: Comparison of the three-dimensional structures of the unliganded Fab and a deoxynucleotide-Fab complex. Proteins 1991;11:159–175.
16. Tanner JJ, Komissarov AA, Deutscher SL. Crystal structure of an antigen-binding fragment bound to single-stranded DNA. J Mol Biol 2001;314:807–822.
17. Calcutt MJ, Kremer MT, Giblin MF, Quinn TP, Deutscher SL. Isolation and characterization of nucleic acid-binding antibody fragments from autoimmune mice-derived bacteriophage display libraries. Gene 1993;137:77–83.
18. Komissarov AA, Marchbank MT, Calcutt MJ, Quinn TP, Deutscher SL. Site-specific mutagenesis of a recombinant anti-single-stranded DNA Fab. Role of heavy chain complementarity-determining region 3 residues in antigen interaction. J Biol Chem 1997;272:26864–26870.
19. Komissarov AA, Deutscher SL. Thermodynamics of Fab/DNA interactions: Contributions of heavy chain complementarity determining region 3. Biochemistry 1999;38:14631–14637.
20. Swanson PC, Ackroyd C, Glick GD. Ligand recognition by anti-DNA autoantibodies. Affinity, specificity, and mode of binding. Biochemistry 1996;35:1624–1633.
21. Ackroyd PC, Cleary J, Glick GD. Thermodynamic basis for sequence-specific recognition of ssDNA by an autoantibody. Biochemistry 2001;40:2911–2922.
22. Cleary J, Glick GD. Mutational analysis of a sequence-specific ssDNA binding lupus autoantibody. Biochemistry 2003;42:30–41.
23. Prewitt SP, Komissarov AA, Deutscher SL, Tanner JJ. Crystallization and Molecular Replacement Studies of a Recombinant Antigen-Binding Fragment Complexed with Single-stranded DNA. Acta Crystallogr D Biol Crystallogr 2000;56:1007–1011.
24. Otwinowski Z, Minor W. Processing of X-ray diffraction data collected in oscillation mode. Methods Enzymol 1997;276:307–326.
25. French GS, Wilson KS. On the treatment of negative intensity observations. Acta Crystallogr A 1978;34:517–525.
26. CCP4. The CCP4 Suite: Programs for protein crystallography. Acta Crystallogr D Biol Crystallogr 1994;50:760–763.
27. Navaza J, Saludjian P. AMoRE: An automated molecular replacement program package. Meth Enzymol 1997;276:581–594.
28. Brünger AT, Adams PD, Clore GM, DeLano WL, Gros P, Grosse-Kunstleve RW, Jiang JS, Kuszewski J, Nilges M, Pannu NS, Read RJ, Rice LM, Simonson T, Warren GL. Crystallography & NMR system: A new software suite for macromolecular structure determination. Acta Crystallogr D Biol Crystallogr 1998;54:905–921.
29. Jones TA, Zou J-Y, Cowan SW, Kjeldgaard M. Improved methods for building protein models in electron density maps and the location of errors in these models. Acta Crystallogr A 1991;47:110–119.
30. Engh RA, Huber R. Accurate bond and angle parameters for X-ray protein structure refinement. Acta Crystallogr A 1991;47:392–400.
31. Jensen LH. Solvent model for protein crystals: on occupancy parameters for discrete solvent sites and the solvent continuum. Acta Crystallogr B 1990;46:650–653.
32. Berman HM, Westbrook J, Feng Z, Gilliland G, Bhat TN, Weissig H, Shindyalov IN, Bourne PE. The Protein Data Bank. Nucleic Acids Res 2000;28:235–242.
33. Zhang YL, Zhang ZY. Low-affinity binding determined by titration calorimetry using a high-affinity coupling ligand: a thermodynamic study of ligand binding to protein tyrosine phosphatase 1B. Anal Biochem 1998;261:139–148.
34. Brünger AT. Assessment of phase accuracy by cross validation: the free R value. Methods and applications. Acta Crystallogr D Biol Crystallogr 1993;49:24–36.
35. Luzzati PV. Traitement statistique des erreurs dans la determination des structures cristallines. Acta Crystallogr 1952;5:802–810.
36. Read RJ. Improved fourier coefficents for maps using phases from partial structures with errors. Acta Crystallogr A 1986;42:140–149.
37. Laskowski RA, MacArthur MW, Moss DS, Thornton JM. PROCHECK: a program to check the stereochemical quality of protein structures. J Appl Crystallogr 1993;26:283–291.
38. Kabat EA, Wu TT, Perry HM, Gottesmann KS, Foeller C. Sequences of proteins of immunological interest. Bethesda, MD: National Institutes of Health; 1991.
39. Martin AC. Accessing the Kabat antibody sequence database by computer. Proteins 1996;25:130–133.
40. Davies DR, Chacko S. Antibody structure. Acc Chem Res 1993;26: 421–427.

41. Amzel LM, Poljak RJ. Three-dimensional structure of immunoglobulins. Ann Rev Biochem 1979;48:961–997.
42. Sobolev V, Sorokine A, Prilusky J, Abola EE, Edelman M. Automated analysis of interatomic contacts in proteins. Bioinformatics 1999;15:327–332.
43. Komissarov AA, Calcutt MJ, Marchbank MT, Peletskaya EN, Deutscher SL. Equilibrium binding studies of recombinant anti-single-stranded DNA Fab. Role of heavy chain complementarity-determining regions. J Biol Chem 1996;271:12241–12246.
44. Ben-Chetrit E, Eilat D, Ben-Sasson SA. Specific inhibition of the DNA-anti-DNA immune reaction by low molecular weight anionic compounds. Immunology 1988;65:479–485.
45. Kowal C, Weinstein A, Diamond B. Molecular mimicry between bacterial and self antigen in a patient with systemic lupus erythematosus. Eur J Immunol 1999;29:1901–1911.
46. Sharma A, Isenberg DA, Diamond B. Crossreactivity of human anti-dsDNA antibodies to phosphorylcholine: clues to their origin. J Autoimmun 2001;16:479–484.
47. Mostoslavsky G, Fischel R, Yachimovich N, Yarkoni Y, Rosenmann E, Monestier M, Baniyash M, Eilat D. Lupus anti-DNA autoantibodies cross-react with a glomerular structural protein: a case for tissue injury by molecular mimicry. Eur J Immunol 2001;31:1221–1227.
48. Gaynor B, Putterman C, Valadon P, Spatz L, Scharff MD, Diamond B. Peptide inhibition of glomerular deposition of an anti-DNA antibody. Proc Natl Acad Sci 1997;94:1955–1960.
49. DeGiorgio LA, Konstantinov KN, Lee SC, Hardin JA, Volpe BT, Diamond B. A subset of lupus anti-DNA antibodies cross-reacts with the NR2 glutamate receptor in systemic lupus erythematosus. Nat Med 2001;7:1189–1193.
50. Sibille P, Ternynck T, Nato F, Buttin G, Strosberg D, Avrameas A. Mimotopes of polyreactive anti-DNA antibodies identified using phage-display peptide libraries. Eur J Immunol 1997;27:1221–1228.
51. Oldstone MB. Molecular mimicry and immune-mediated diseases. FASEB J 1998;12:1255–1265.
52. Pewzner-Jung Y, Simon T, Eilat D. Structural elements controlling anti-DNA antibody affinity and their relationship to anti-phosphorylcholine activity. J Immunol 1996;156:3065–3073.
53. Ray SK, Putterman C, Diamond B. Pathogenic autoantibodies are routinely generated during the response to foreign antigen: a paradigm for autoimmune disease. Proc Natl Acad Sci USA 1996;93:2019–2024.
54. Yin J, Beuscher AEt, Andryski SE, Stevens RC, Schultz PG. Structural plasticity and the evolution of antibody affinity and specificity. J Mol Biol 2003;330:651–656.
55. Esnouf RM. An extensively modified version of MolScript that includes greatly enhanced coloring capabilities. J Mol Graph Model 1997;15:132–134.
56. Merritt EA, Murphy MEP. Raster3D Version 2.0: A program for photorealistic molecular graphics. Acta Crystallogr D Biol Crystallogr 1994;50:869–873.
57. DeLano WL. The PyMOL molecular graphics system (http://www.pymol.org). 2002.